MLM--3951(OP)

DE89 014734

MLM-3371(OP)

CONF-8905167--1

AN AUGER SPUTTER PROFILING STUDY OF NITROGEN AND OXYGEN ION IMPLANTATIONS IN TWO TITANIUM ALLOYS

B. D. Barton, EG&G Mound Applied Technologies, Miamisburg, OH 45343

L. E. Pope, Sandia National Laboratories, Albuquerque, NM 87185

T. N. Wittberg, University of Dayton Research Institute, Dayton, OH 45469

ABSTRACT

Samples of two titanium alloys, Ti-6Al-4V and Ti-15V-3Cr-3Sn-3Al, were ion implanted with a combination of nitrogen (N+) and oxygen (O+). For each alloy, implantation parameters were chosen to give implanted nitrogen concentrations of approximately 10 or 50 atomic percent, from a depth of 100 nanometers to a depth of 400 nanometers. In all but one case, dual energy (200 keV and 90 keV) implantations of nitrogen were used to give a relatively uniform nitrogen concentration to a depth of 300 nanometers. In each case, oxygen was implanted at 35 keV, following the nitrogen implantation, to give an oxygen-enriched region near the surface. The implanted samples were then examined by Auger electron spectroscopy (AES) combined with argon ion sputtering. In order to determine the stoichiometry of the nitrogen implanted regions, it was necessary to determine the N(KVV) contribution to the overlapping N(KVV) and Ti(LMM) Auger transitions. It was also necessary to correct for the ion-bombardment-induced compositional changes which have been described in an earlier study of titanium nitride thin films. The corrected AES depth profiles were in good agreement with theoretical predictions.

I. INTRODUCTION

Since 1973, researchers have investigated the effects of ion implantation of nitrogen into ferrous alloys [1]. In many cases, they found significant improvements in surface mechanical properties, such as hardness and wear resistance. Vardiman and Kant extended nitrogen ion implantation to the case of Ti-6Al-4V, a technologically important titanium alloy widely used for aerospace and medical applications [2]. They found that improvements in fatigue life of Ti-6Al-4V could be obtained with either carbon or nitrogen implantation. Oliver, Hutchings and Pethica found that the hardness of Ti-6Al-4V could be increased by a factor of 2, and the wear resistance by a factor of up to 500 by nitrogen implantation [3]. In detailed wear testing and analysis, Hutchings and Oliver found that the improvement in wear resistance and the lowered coefficient of friction in nitrogen-implanted Ti-6Al-4V were associated with the formation of an oxide layer formed during wear of the implanted surface, and that the formation of the oxide layer was dependent upon the presence of implanted nitrogen [4].

The presence of oxygen appears to be critical to the wear resistance of nitrogen implanted Ti-6Al-4V. No increase in wear resistance is found in cases where the oxide film is absent [2]. Pons, Pivin and Farges found that when there is no oxide layer on the TiN surface, the hard nature of this material eventually leads to severe abrasive wear [5]. Since the development of a lubricious oxide surface will not occur in oxygen-deficient environments, it may be necessary to tailor the surface composition by implantation of both nitrogen and oxygen.

AES depth profiling has been used to study ion implant distributions in various materials. Steel surfaces implanted with Ti [6] or with a combination of Ti and C [7] have been studied. AES has also been used to study iron or steel surfaces implanted with N [8] or with a combination of N and Ti [9]. In one of these studies [8], AES depth profiles were correlated with

wear test data in developing a model for how implanted ions modify wear properties.

In the present study two titanium alloys, Ti-6Al-4V and Ti-15V-3Cr-3Sn-3Al, were chosen for examination. Samples were subjected to high dose ion implantation with nitrogen and oxygen. The implanted samples were then analyzed with AES depth profiling in order to determine the implanted ion distributions. The AES results were compared with theoretical ion distributions given by a commercial software package [10].

II. EXPERIMENT

A. Sample Preparation

Ti-6Al-4V bars were received from the Earle M. Jorgensen Company in the mill-annealed condition. The Ti-15V-3Cr-3Sn-3Al bars that were received from Titanium Metals Corporation had been solution annealed and aged at 482°C for 16 hours. Circular disks, 3.02 centimeters in diameter by 1.3 millimeters thick, were cut from these bars. Ti-6Al-4V disks were mechanically lapped to a surface finish of from 0.2 to 0.3 micrometers, and Ti-15V-3Cr-3Sn-3Al disks were lapped to a surface finish of 0.4 micrometers. Chemical compositions for the two alloys are given in Table 1, with nominal compositional ranges for Ti-6Al-4V, and values for Ti-15V-3Cr-3Sn-3Al taken from the certificate of analysis supplied by the manufacturer. Prior to being mounted for ion implantation, the disks were rinsed in trichloroethylene, washed ultrasonically in a detergent solution, rinsed in deionized water, and rinsed in isopropanol, in order to remove superficial surface contaminants.

The titanium alloys examined in this study are different with respect to both surface mechanical properties and microstructure, and represent two extremes of titanium alloy metallurgy. Differences were evident in preparing samples for microscopic examination. Samples of each alloy were polished in a series of steps, ending with 0.03 μm silica. It was difficult to obtain good results in polishing the Ti-6Al-4V specimen, due

to grain pull-out and the ductile nature of the material. Profilometry of the polished samples indicated a surface finish of <50 nm for the Ti-15V-3Cr-3Sn-3Al specimen, whereas the surface of the Ti-6Al-4V specimen had surface features as deep as 400 nm. The Ti-6Al-4V specimen was etched in 25% HNO_3/2% HF at 54° C, to reveal the microstructure shown in Figure 1a. The fine-grained lamellar microstructure shown is typical of this mill-annealled alpha-beta processed titanium alloy. The use of the same chemical etchant with the beta-stabilized Ti-15V-3Cr-3Sn-3Al resulted in a darkening of the specimen with low grain contrast and was therefore not useful for revealing the microstructure. Instead, examination was made of the bottom of an argon sputter-etched crater to reveal the coarse-grained polygonal microstructure shown in Figure 1b.

B. Ion Implantation

The intent of the implantation work was to produce deep implantations that would be relatively level through the use of multiple energy implantation, with a relatively thick nitrogen-implanted region under a thinner oxygen-enriched region. In order to achieve these goals, a commercial software package [10] was used for theoretical modeling. The software is based primarily on ZBL transport theory, using a formulation by Biersack [11]. In general, the calculated distribution of implanted ions is a four moment Pearson distribution. The software takes into account sputtering which occurs concurrently with ion implantation, and which ultimately limits the implanted ion concentration at sufficiently high fluence.

Sputtering coefficients used in the calculations are interpolated from data compiled by Matsunami et. al. for a range of ions, targets, and energies [12]. A more detailed discussion of similar theoretical modeling software was recently presented by Bunker and Armini [13]. By means of the software, three nitrogen implant models were chosen: a) 200 keV maximum energy with implanted ion concentrations on the order of 50 atomic %; b) 200 keV maximum energy with implanted ion concentrations on the

order of 10 atomic %; and c) 90 keV maximum energy with implanted ion concentrations on the order of 10 atomic %. These cases are henceforth referred to as (200 keV, 50 atomic %), etc. Models were calculated for the Ti-6Al-4V target material only, since the target materials are sufficiently similar that little difference would be expected in the implanted ion distributions. Implant parameters derived from the theoretical models, along with the associated sputtering coefficients are shown in Table 2. Representative theoretical depth profiles are shown in Figure 2, for the (200 keV, 50 atomic %) and (90 keV, 10 atomic %) cases. The (200 keV, 10 atomic %) case is similar to the (200 keV, 50 atomic %) case, except for the dose levels at each energy. Implantations consisted of a 200 keV nitrogen implant, followed by a 90 keV nitrogen implant, followed by a 35 keV oxygen implant. In one case, only the 90 keV nitrogen implant followed by the 35 keV oxygen implant was used. The titanium alloy disks were mounted to an adapter plate which could accept seven specimens. The adapter plate was in turn mounted to a fixture supplied as standard equipment by the implanter manufacturer. An aluminum foil gasket was used between the adapter plate and the implant fixture to assure good thermal transport.

Ion implantations were carried out on a Varian/Extrion 350D ion implanter, equipped with dual research end stations. The research cube fixture, used for mounting specimens, was outfitted with a heat exchanger connected to a refrigerated fluid recirculator, to allow control of specimen temperature rise due to ion beam heating. The implanter was further equipped with a residual gas analyzer inserted into the end station vacuum system. Thus, gas composition within the implanter vacuum system could be monitored while implantation was taking place. Pressures in the end station vacuum system were maintained below 3×10^{-4} Pa during the implantations. The three implantation cases were implanted concurrently, by periodically stopping implantation and removing selected specimens. This procedure allowed all of the cases to be implanted under similar

conditions, but required periodically exposing the sample set to laboratory air. Two samples each of the two alloys were implanted under (200 keV, 50 atomic %) conditions; one sample of each alloy was implanted under (200 keV, 10 atomic %) conditions; and one sample of Ti-6Al-4V only was implanted under (90 keV, 10 atomic %) conditions. Target temperatures measured during the implantations ranged from 258 to 310° K, with an average value of 290° K. Ion current densities fell in the range of 3 to 4 $\mu amps/cm^2$ for N+ implantation, and 0.7 to 0.8 $\mu amps/cm^2$ for O+ implantation.

C. AES Depth Profiling Analysis

Depth profiling of the implanted titanium alloy specimens was accomplished with a modified Varian model 981-2707 Auger electron spectrometer, interfaced to a DEC LSI minicomputer for data acquisition. Data was transferred to a VAX 11/780 minicomputer where processing was done using custom software. Samples were masked for depth profiling with aluminum foil containing a 3 mm diameter hole to limit sputtering to the center of each specimen. The vacuum chamber was backfilled with argon to a pressure of 7×10^{-3} Pa and a Varian model 981-2043 ion gun operating at 2 kV was used for sputtering. A 5 kV electron beam rastered over an area of 0.01 mm^2 was used for analysis. There was a modulation of 10 eV peak-to-peak on the CMA. Relative sensitivity factors used were: S(C) = 4.0, S(O) = 1.0, S(N) = 2.4, S(Ti) = 1.9, S(V) = 2.6, and S(Al) = 2.5, as previously determined for this instrument under these experimental conditions.

III. AES DEPTH PROFILING RESULTS

A typical surface scan is shown in Figure 3, for the (200 keV, 50 atomic %) specimen of Ti-15V-3Cr-3Sn-3Al. Surface scans for Ti-6Al-4V were similar, but without noticeable contributions from vanadium.

As is evident in Figure 3, the Auger N KLL signal and Ti LMM signals at 380 eV overlap. At least two methods are in

general use for resolving the nitrogen and titanium signals, based on the signals at 380 eV and the Ti LMV signal at 418 eV. Dawson and Tzatzov attributed the full peak-to-peak amplitude of the 418 eV signal to titanium, and obtained the nitrogen intensity by subtracting the portion of the peak at 380 eV attributable to titanium [14]. Sundgren, Johansson, and Karlsson derived the nitrogen signal from the positive excursion of the 380 eV peak and the titanium signal from the negative excursion of the 418 eV peak [15]. The method of Sundgren et al. was used to resolve the titanium and nitrogen intensities in the present study.

Auger depth profiles for the five cases are shown in Figure 4. In order to convert sputter etch times into depth units, it was necessary to determine sputter etching rates for the five cases. Etch rates for some materials had been previously determined. A value of 5.0 nm/min had been found for anodically grown rutile (TiO_2) films [16], and a value of 5.6 nm/min for a TiN film on silicon.

Polished samples of unimplanted Ti-6Al-4V and Ti-15V-3Cr-3Sn-3Al were sputter etched and the crater depths measured by profilometry. The values obtained were 8 $\pm$ 1 nm/min for Ti-6Al-4V and 5.8 $\pm$ 0.5 nm/min for Ti-15V-3Cr-3Sn-3Al. The larger uncertainty in the sputtering rate for Ti-6Al-4V is due to the greater variation in the crater profilometer trace for this material. Microscopic examination of the sputtered craters revealed a relatively flat, uniform surface for Ti-15V-3Cr-3Sn-3Al, whereas the sputtered surface of the Ti-6Al-4V had a sponge-like appearance, indicating differential sputtering of grain structures had occurred. Thus, we may infer that the measured rate of 8 nm/min for Ti-6Al-4V represents a composite of the rates for rapidly etched phases(s) and for the more slowly etched phase(s).

Based on these measurements, then, the following sputter etch rates were used for depth scaling in Figure 4: a) 5.6

nm/min for the two (200 keV, 50 atomic %) cases (Figures 4a and 4b), since the compositions of these were believed to be similar to TiN; b) 5.8 nm/min for the (200 keV, 10 atomic %) case of Ti-15V-3Cr-3Sn-3Al (Figure 4d); and c) 8 nm/min for the two 10 atomic % cases of Ti-6Al-4V. The derived depth scales were also used for Figures 5 and 6.

The (200 keV, 50 atomic %) depth profiles for Ti-6Al-4V and Ti-15V-3Cr-3Sn-3Al (Figures 4a and b) are similar. From the near surface to about 90 nm is a region of variable composition of the form TiO_xN_y with less than 10 atomic % contribution from C. The oxygen profile shows a local minimum due to the overlap of contributions from implanted oxygen and from the native or surface oxide. The Ti-6Al-4V specimen has a surface rich in aluminum oxide, but the Ti-15V-3Cr-3Sn-3Al does not show this feature.

The region from 90 nm to 400 nm is a nitrogen-rich region, with a (Ti + V)/N ratio of approximately one, suggesting near stoichiometric formation of titanium nitride. Carbon concentrations, in the Ti-15V-3Cr-3Sn-3Al specimen, appear to increase monotomically with depth. This unexpected feature is probably the result of the gettering of trace hydrocarbons from the AES vacuum system. The two (200 keV, 10 atomic %) cases (Figures 4c and d) are again quite similar. A bimodal nitrogen signal is evident from 100 nm to 400 nm, with a maximum concentration of about 20 atomic %, twice as high as predicted. The higher than expected value is believed to be due to the variation in Auger sensitivity for nitrogen in TiN_x films, as has been discussed by Burrow, Morgan, and Ellwanger [17]. This discrepancy will be discussed in more detail later. The implanted oxygen appears as a broad shoulder extending from the native oxide. The carbon signal roughly parallels the oxygen signal, suggesting that some recoil implantation of carbon may have occurred. Residual gas analyses, recorded during oxygen implantation, indicated elevated levels of carbon monoxide in the vacuum system. Carbon monoxide was evolved from the ion source when carbon dioxide was used as a source gas. Clean titanium surfaces are known to be efficient scavengers of carbon, nitrogen, and oxygen. Thus, the source of

the recoil-implanted carbon (and oxygen) was likely an adsorbed layer of carbon monoxide and hydrocarbons. The (90 keV, 10 atomic %) case is very similar to the (200 keV, 10 atomic %) cases, except for a unimodal nitrogen distribution rather than a bimodal nitrogen distribution.

IV. COMPARISON OF AES RESULTS WITH MODEL

Theoretical depth profiles are compared with AES profiles in Figure 5, for nitrogen and oxygen under (200 keV, 50 atomic %) conditions; and in Figure 6, for nitrogen under 10 atomic % conditions. In these comparisons, oxygen profiles are plotted as atomic % and nitrogen profiles as N/Ti ratios, as a matter of computational convenience.

Deviations from theory in high fluence implantation can arise due to ion-enhanced diffusion, ion-enhanced segregation, surface contraction or expansion, and the changing nature of sputtering coefficients and electronic and nuclear stopping powers. Despite these limitations, good qualitative agreement is seen between the theory and AES measurement. The oxygen profiles in Figure 7 are in excellent agreement with theory, except for the contribution from the native oxide, which was not included in the model. The as-measured AES nitrogen profiles in Figure 7 are broader than predicted, with substantial tailing in the case of the Ti-15V-3Cr-3Sn-3Al sample. The as-measured AES nitrogen profiles in Figure 8 differ from theoretical by a factor of about 2.5 in magnitude. Most of the discrepancies noted are due to a variation in Auger sensitivity with composition. Burrow, Morgan, and Ellwanger examined samples of TiN_x films, where x = 0 to 1.2, by Rutherford backscattering (RBS), x-ray photoelectron spectroscopy (XPS), and Auger electron spectroscopy [17]. These authors found a nonlinear variation in sensitivity with composition for both XPS and AES, compared with RBS, which was used as a reference. XPS and AES share the common feature of using sputtering for depth profiling, while RBS depends upon backscattering of high energy helium ions and does not require sputtering for

depth profiling. The authors reached the conclusion that the variation in sensitivity observed
was due to ion-induced compositional changes which occurred during sputtering for TiN_x films, where $x \leq 0.3$. They presented a curve relating N/Ti ratios measured by AES to N/Ti ratios measured by RBS. The data of Burrow is well-represented by a third order polynomial of the form

$$y = \Sigma a_i \, x^i \qquad (i = 0,3),$$

where y is the corrected N/Ti value,
x is the original N/Ti value,
$a_0 = -0.071207$,
$a_1 = 1.0544$,
$a_2 = 2.5247$, and
$a_3 = 2.6996$.

Additive corrections, ranging from 0.014 to 0.050, were made to the corrected profiles as required to give non-negative values at large depths. The effect of the Burrow correction was to lower peak concentrations by a factor of about three, from 20 atomic % to about 6 atomic %, in the case of the low fluence (10 atomic %) implants. When the same corrections were applied to the high dose cases, peak concentrations changed very little, but the widths of the implanted zones decreased, and the tailing was reduced. In Figure 5, corrected profiles are shown only for values of N/Ti <0.8, since corrections are small for higher values of N/Ti.

Even after making corrections for AES sensitivity variations, some discrepancies exist with respect to the depth scale for the (200 keV, 10 atomic %) case of Ti-15V-3Cr-3Sn-3Al. A sputtering rate of 5.8 nm/min was measured for unimplanted Ti-15V-3Cr-3Sn-3Al, and was used to define the depth scale for the

(200 keV, 10 atomic %) case of this alloy. A sputter rate of 8 nm/min would give agreement with theory and with the Ti-6Al-4V cases. We recall that phases present in the biphasic alpha-beta Ti-6Al-4V were found to sputter at different rates. Pons et al. noted the complete disappearance of the beta phase in nitrogen-implanted Ti-6Al-4V by the time 15 atomic % N was reached [5]. Hutchings also noted a reduction in the volume of beta phase in nitrogen-implanted Ti-6Al-4V [19]. Many materials undergo phase transformations during ion bombardment, in some cases changing to amorphous structures. In nitrogen-implanted Ti-6Al-4V, the alloy does not become amorphous, but transforms to single phase alpha. One may expect some change in microstructure to occur similarly in nitrogen implanted Ti-15V-3Cr-3Sn-3Al. Thus, it is possible that the implanted Ti-15V-3Cr-3Sn-3Al has undergone a phase transformation, such that the final phase of implanted Ti-15V-3Cr-3Sn-3Al has a sputter rate similar to that of the final alpha phase of implanted Ti-6Al-4V.

V. CONCLUSIONS

In the present study, two titanium alloys have each been implanted with high levels of both oxygen and nitrogen. The intention has been to create low friction surfaces similar to those described in other studies. AES depth profiling has been used to determine the distributions of the implanted ions. The profiles show that surface layers ~90 mm thick are formed which contain oxygen, carbon, and nitrogen. Beneath these surface layers are relatively thick regions of nitrogen enrichment. In order to quantitatively determine the nitrogen profiles from the AES data it was necessary to correct for the ion bombardment induced compositional changes which were measured in a combined RBS, AES, and XPS study of thin titanium nitride films [17]. The corrected AES depth profiles are generally in good agreement with theoretical predictions.

ACKNOWLEDGEMENTS

The authors wish to thank D.W. Brohard and M.W. Donnelly for assistance in preparing the test specimens and S.E. Swallom for the profilmetry measurements.

REFERENCES

1. S. T. Picraux, Annual Review of Material Science, 14, 335 (1984).

2. R. G. Vardiman and R. A. Kant, Journal of Applied Physics, 53 (1), 690 (1982).

3. W. C. Oliver, R. Hutchings, and J. B. Pethica, Metallugurical Transactions A, 15A, 2221 (1984).

4. R. Hutchings and W. C. Oliver, Wear, 92, 143 (1983).

5. F. Pons, J. C. Pivin, and G. Farges, J. Mat. Res., 2, 580 (1987).

6. I. L. Singer and R. A. Jeffries, J. Vac. Sci. Technol. A1 317 (1983).

7. F. M. Kustas, M. S. Misra, and W. T. Tack, J. Vac. Sci. Technol. A4 2885 (1986).

8. T. J. Sommerer, E. B. Hale, K. W. Burris, and R. A. Kosher, Materials Sci. and Eng. 69, 149 (1985).

9. I. L. Singer, Vacuum 34, 853 (1984).

10. Profile Code, Implant Sciences, Danvers, MA.

11. J. P. Biersack, "The Calculation of Ion Ranges in Solids with Analytic Solutions," in Ion Implantation Techniques, H. Ryssel (ed.), Springer Series in Electrophysics, Volume 10, Springer Verlag, 1982.

12. N. Matsunami, Y. Yamamura, Y. Itikawa, N. Itoh, Y. Kazumata, S. Miyagawa, K. Morita, R. Shimizu, and H. Tawara, " Atomic Data and Nuclear Data Tables, 31, 1 (1984).

13. S. N. Bunker and A. J. Armini, "Modeling of Concentration Profiles from Very High Dose Ion Implantation," Proceedings of the Sixth International Conference on Ion Beam Modification of Materials, Tokyo, Japan, 1988.

14. P. T. Dawson and K. K. Tzatzov, Surface Science, 149, 105-118 (1985).

15. J. E. Sundgren, B. O. Johansson, and S. E. Karlsson, Surface Science, 128, 265-280 (1983).

16. T. N. Wittberg, J. D. Wolf, R. G. Keil, and P. S. Wang, Journal of Vacuum Science and Technology A, 1(2), 475 (1983).

17. B. J. Burrow, A. E. Morgan, and R. C. Ellwanger, Journal of Vacuum Science and Technology A, 4(6), 2463 (1986).

18. R. Hutchings, Mat. Sci. and Eng. 69, 129 (1985).

Table 1. Compositions of titanium alloys.

Ti-6Al-4V

density = 4.35 ± 0.01 g/cc; atomic density = 5.71×10^{22} atoms/cc

	Ti	Al	V
weight %	bal.	5.5-6.75	3.5-4.5
atomic %	86.2	10.2	3.6

Note: atomic density and composition based on nominal 90% Ti, 6% Al, 4% V.

Ti-15V-3Cr-3Sn-3Al

density = 4.70 ± 0.01 g/cc; atomic density = 5.88×10^{22} atoms/cc

	Ti	V	Cr	Sn	Al
weight %	75.6	15.7	3.0	2.7	3.0
atomic %	75.9	14.8	2.8	1.1	5.3

Table 2. Implant parameters derived from theoretical modelling

Target: Ti-6Al-4V

S = sputtering coefficient

Case	Ion	Energy (keV)	Fluence (ions/cm^2)	S
200 keV, 50	N^+	200	1.2×10^{18}	0.101
atomic %	N^+	90	5.4×10^{17}	0.197
	O^+	35	3×10^{17}	0.482
Sputtering loss = 63.9 nm				
200 keV, 10	N^+	200	1.4×10^{17}	0.101
atomic %	N^+	90	7×10^{16}	0.197
	O^+	35	3.8×10^{16}	0.482
Sputtering loss = 7.9 nm				
90 keV, 10	N^+	90	1×10^{17}	0.197
atomic %	O^+	35	3.4×10^{16}	0.482
Sputtering loss = 6.2 nm				

Figure Captions

Figure 1. Optical micrographs of a.) Ti-6Al-4V and b.) Ti-15V-3Cr-3Sn-3Al.

Figure 2. Theoretical depth profiles for nitrogen and oxygen implantation into Ti-6Al-4V; a.) 200 keV maximum energy, 50 atomic %, and b.) 90 keV maximum energy, 10 atomic %.

Figure 3. AES surface scan of Ti-15V-3Cr-3Sn-3Al sample implanted under (200 keV, 50 atomic %) conditions.

Figure 4. AES depth profiles for titanium alloy samples implanted with nitrogen and oxygen: a.) Ti-6Al-4V (200 keV, 50 atomic %); b.) Ti-15V-3Cr-3Sn-3Al (200 keV, 50 atomic %); c.) Ti-6Al-4V (200 keV, 10 atomic %); d.) Ti-15V-3Cr-3Sn-3Al (200 keV, 10 atomic %); and e.) Ti-6Al-4V (90 keV, 10 atomic %).

Figure 5. Comparison of theoretical depth profiles and AES depth profiles for combined 200 keV, 50 atomic % N implant and 35 keV 0 implant: a.) nitrogen profile, Ti-6Al-4V; b.) oxygen profile, Ti-6Al-4V; c.) nitrogen profile, Ti-15V-3Cr-3Sn-3Al; and d.) oxygen profile, Ti-15V-3Cr-3Sn-3Al.

Figure 6. Comparison of theoretical nitrogen profiles with AES nitrogen profiles for: a.) Ti-6Al-4V, 200 keV, 10 atomic %; b.) Ti-15V-3Cr-3Sn-3Al, 200 keV, 10 atomic % and c.) Ti-6Al-4V, 90 keV, 10 atomic %.

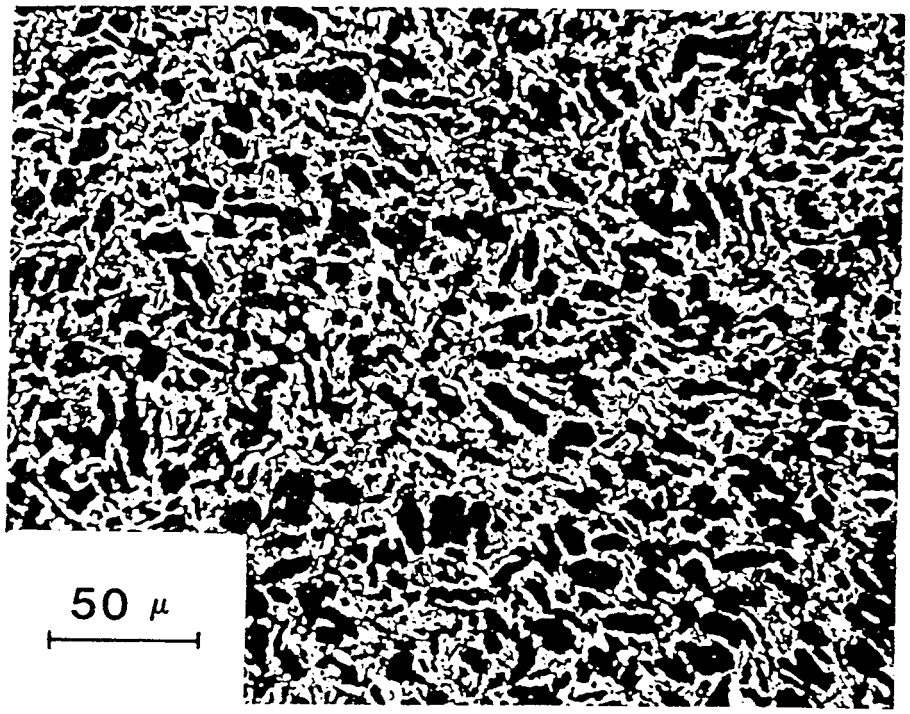

1a.

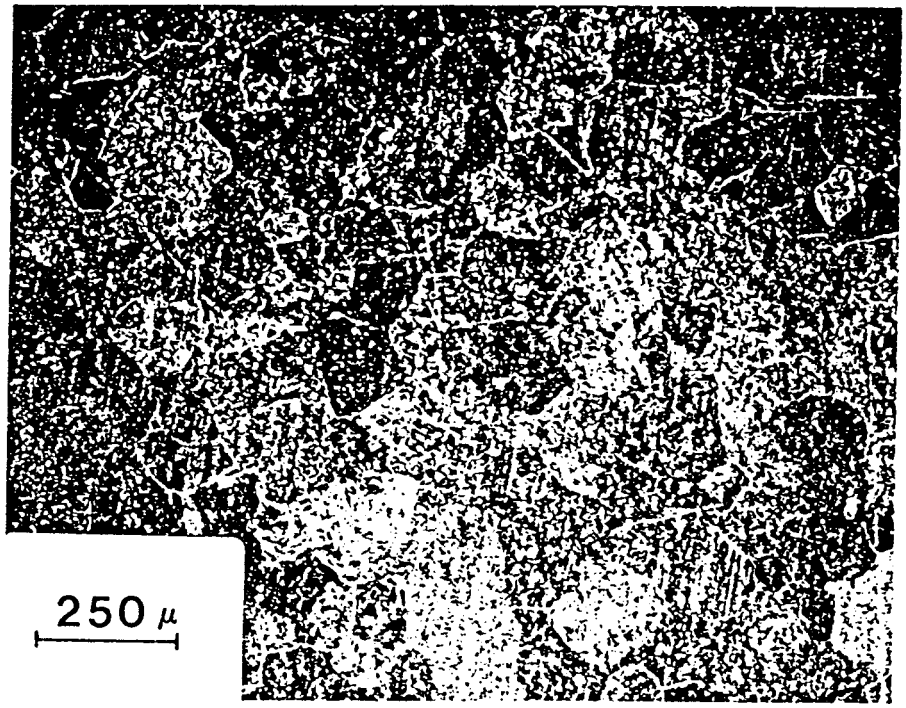

1b.

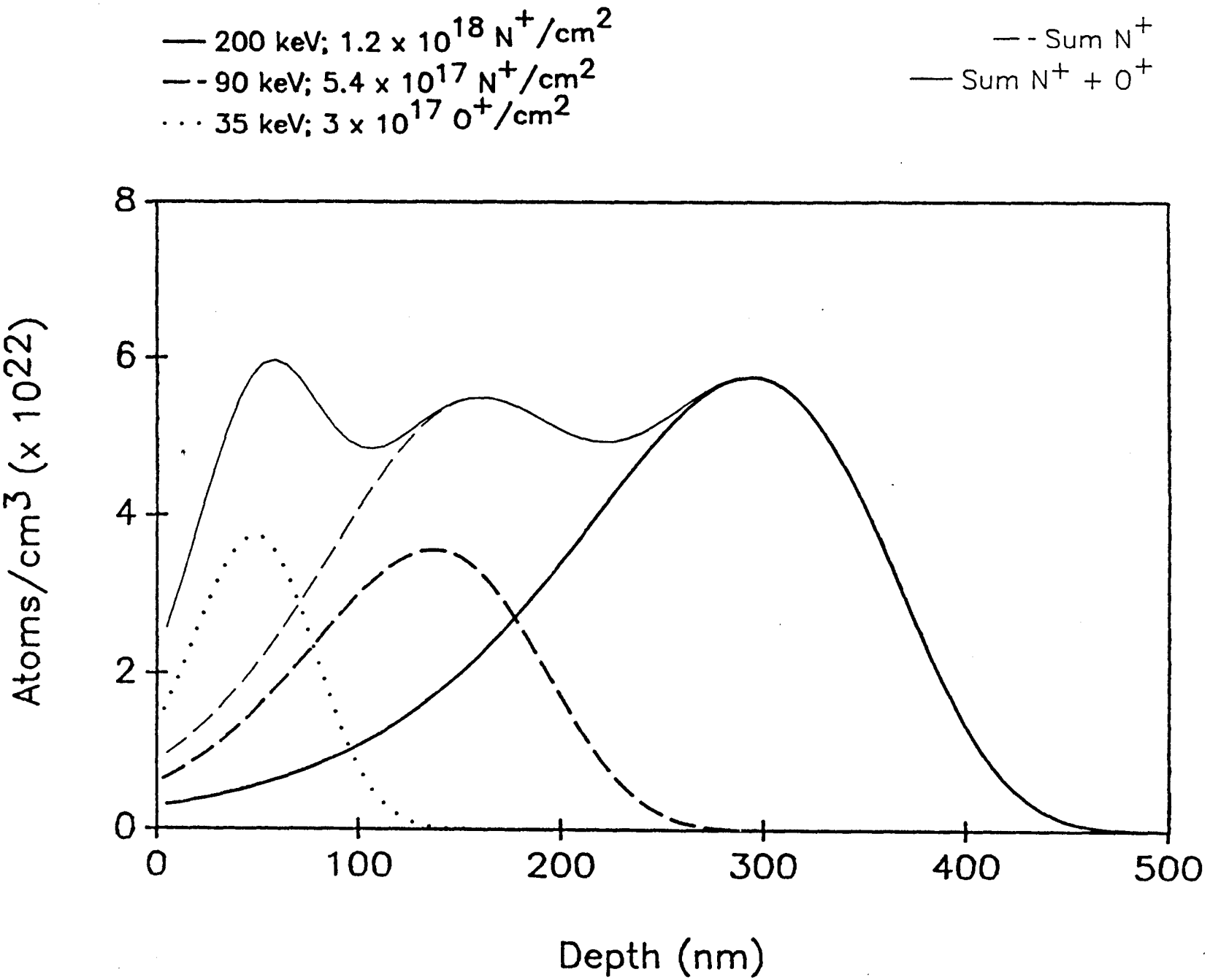
— 200 keV; 1.2 x 10^18 N+/cm2
— - 90 keV; 5.4 x 10^17 N+/cm2
· · · 35 keV; 3 x 10^17 O+/cm2
— - Sum N+
— Sum N+ + O+
Atoms/cm3 (x 1022)
8
6
4
2
0
0
100
200
300
400
500
Depth (nm)

2a

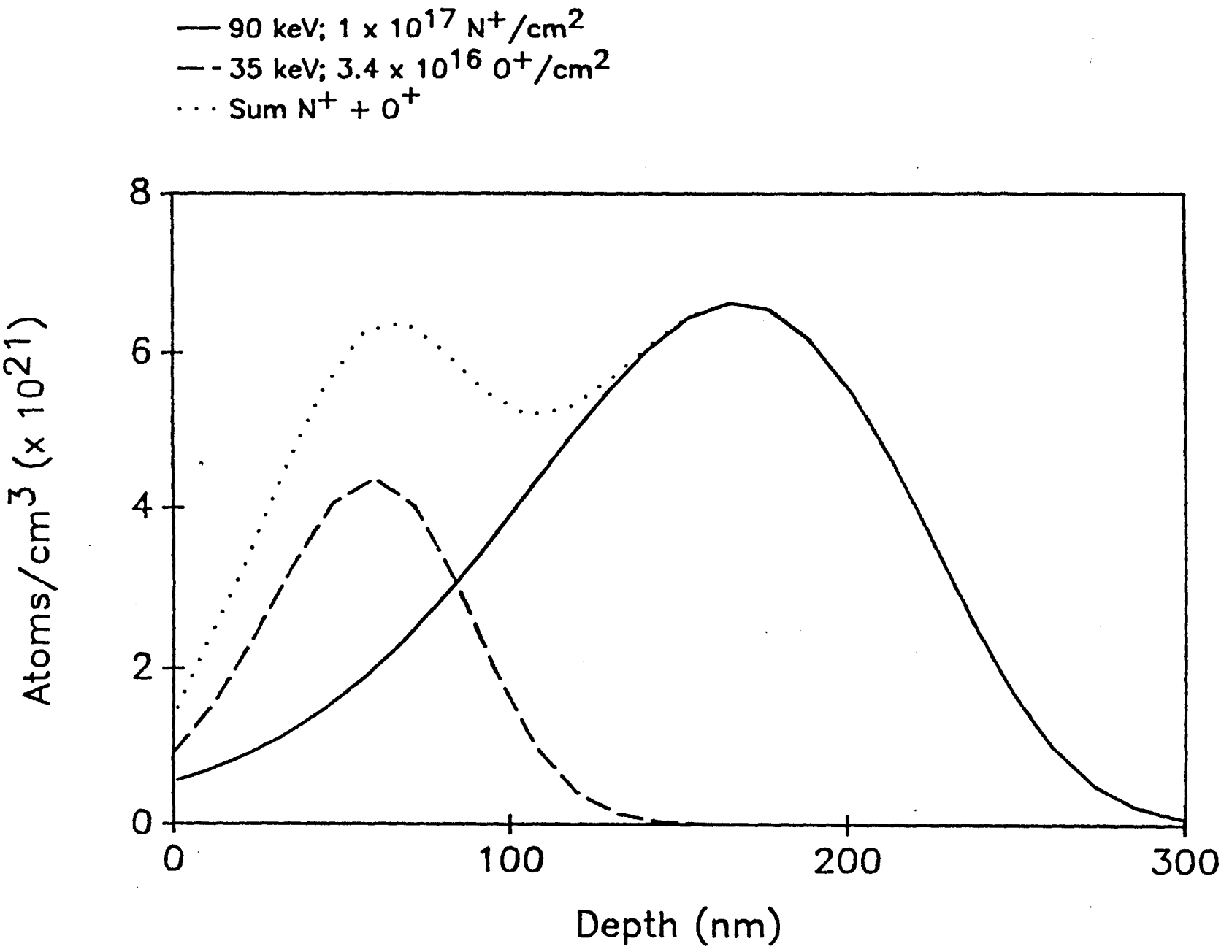
— 90 keV; 1 x 10^17 N+/cm2
— - 35 keV; 3.4 x 10^16 O+/cm2
· · · Sum N+ + O+
Atoms/cm3 (x 10^21)
8
6
4
2
0
0
100
200
300
Depth (nm)

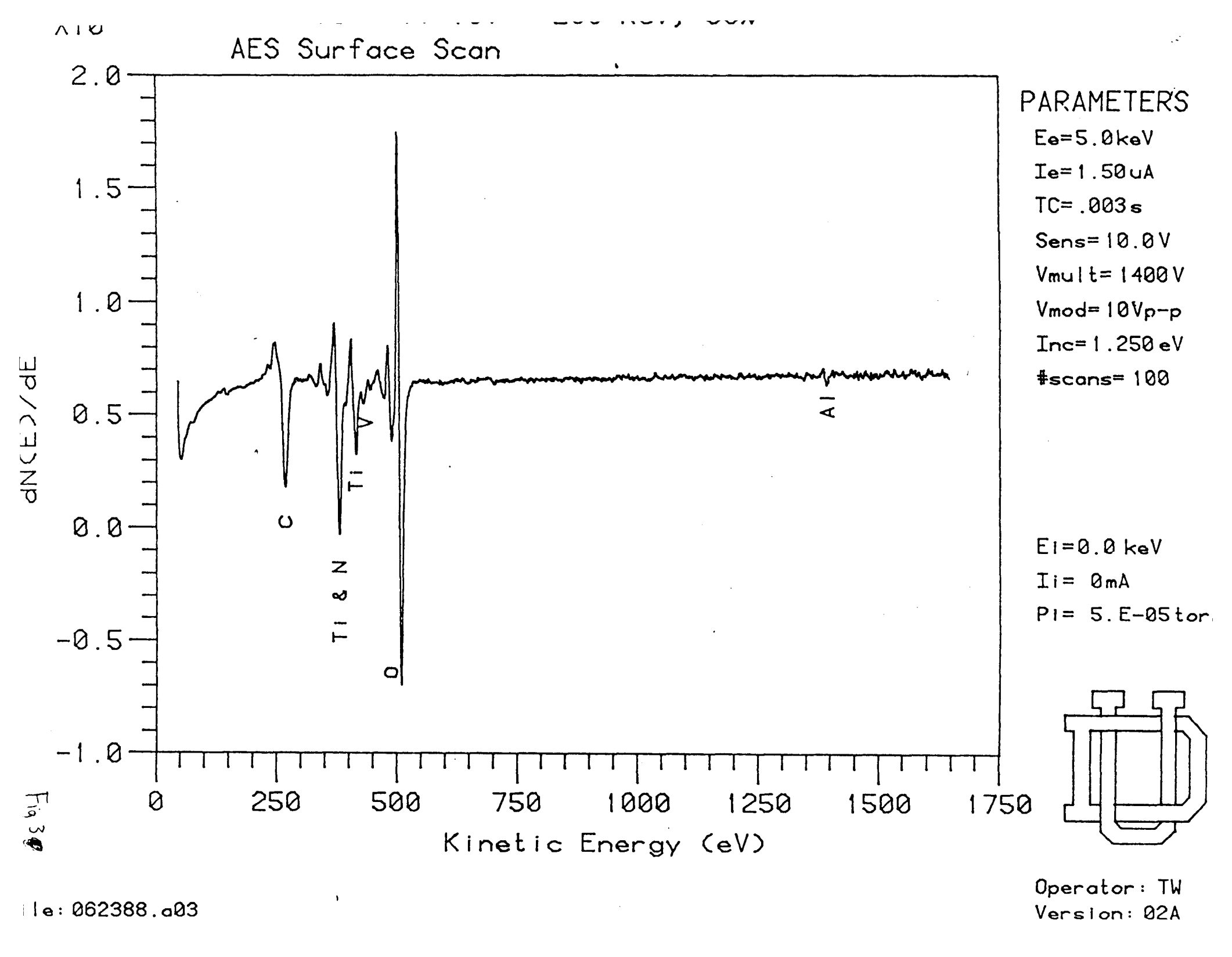
AES Surface Scan
2.0
1.5
1.0
0.5
0.0
-0.5
-1.0
dN(E)/dE
0
250
500
750
1000
1250
1500
1750
Kinetic Energy (eV)
C
Ti & N
Ti
V
O
Al
PARAMETERS
Ee=5.0keV
Ie=1.50uA
TC=.003s
Sens=10.0V
Vmult=1400V
Vmod=10Vp-p
Inc=1.250eV
#scans=100
Ei=0.0 keV
Ii= 0mA
Pi= 5.E-05tor
Operator: TW
Version: 02A
File: 062388.a03

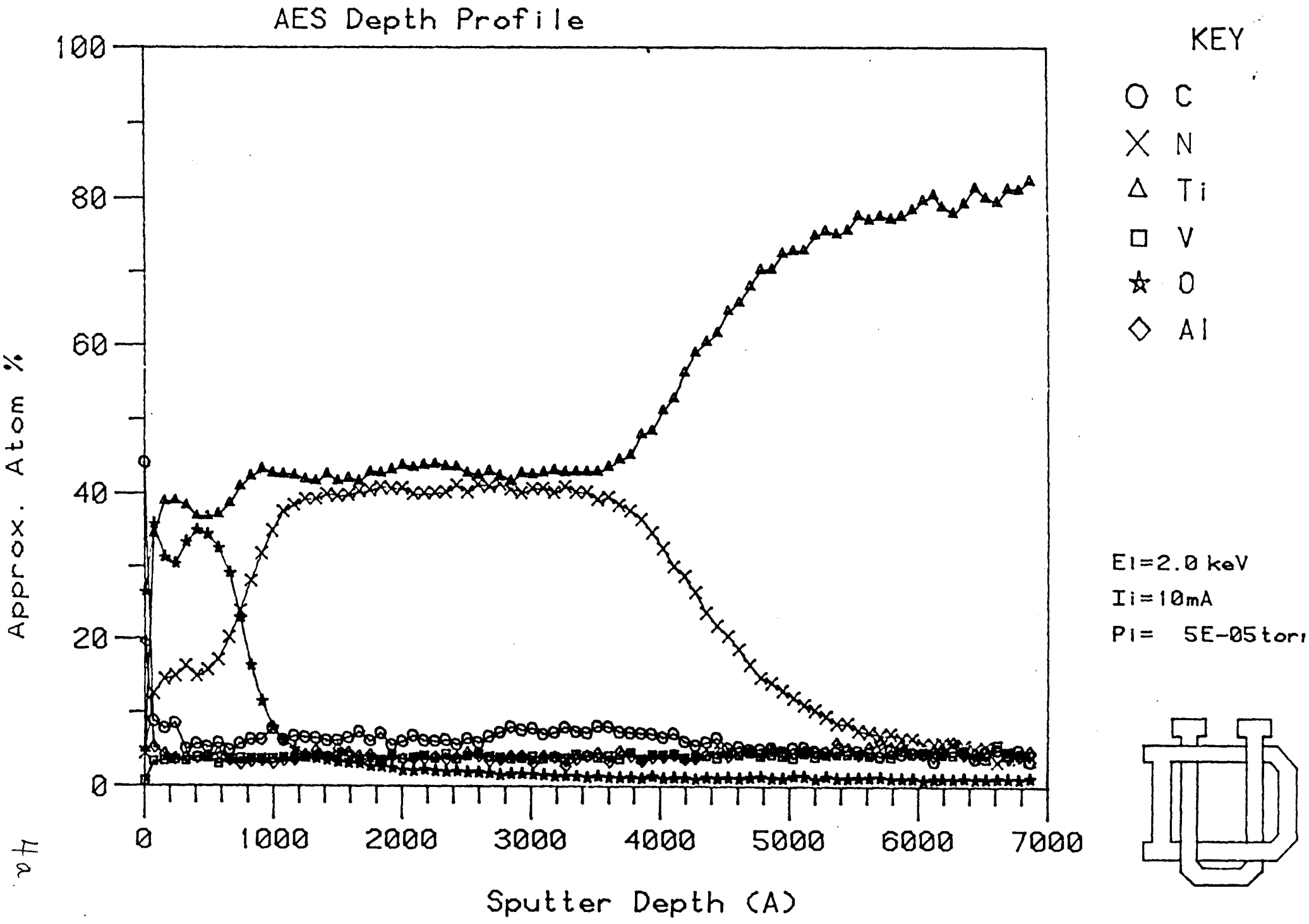

File: 062788.A02

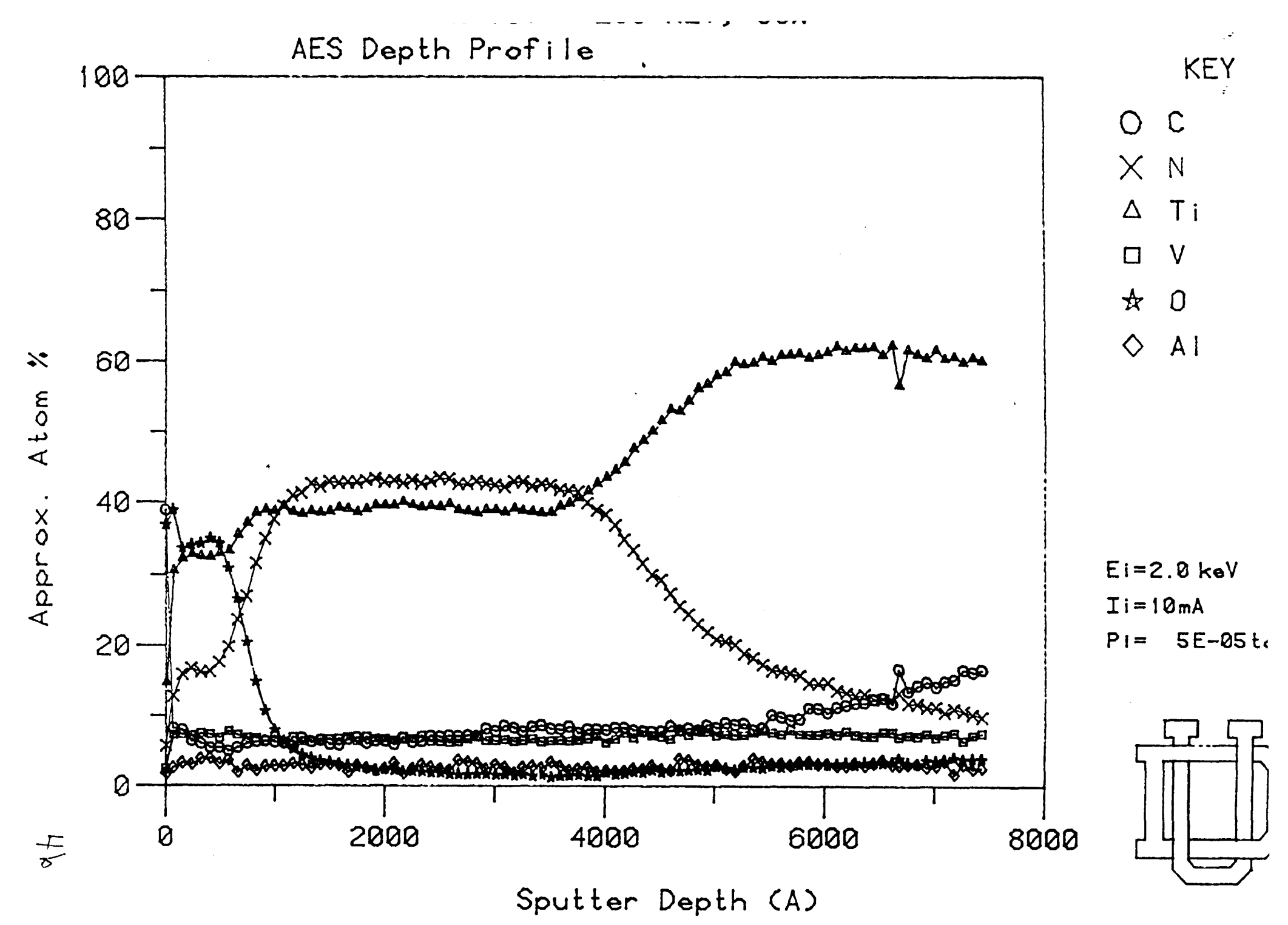

File: 062388.A04

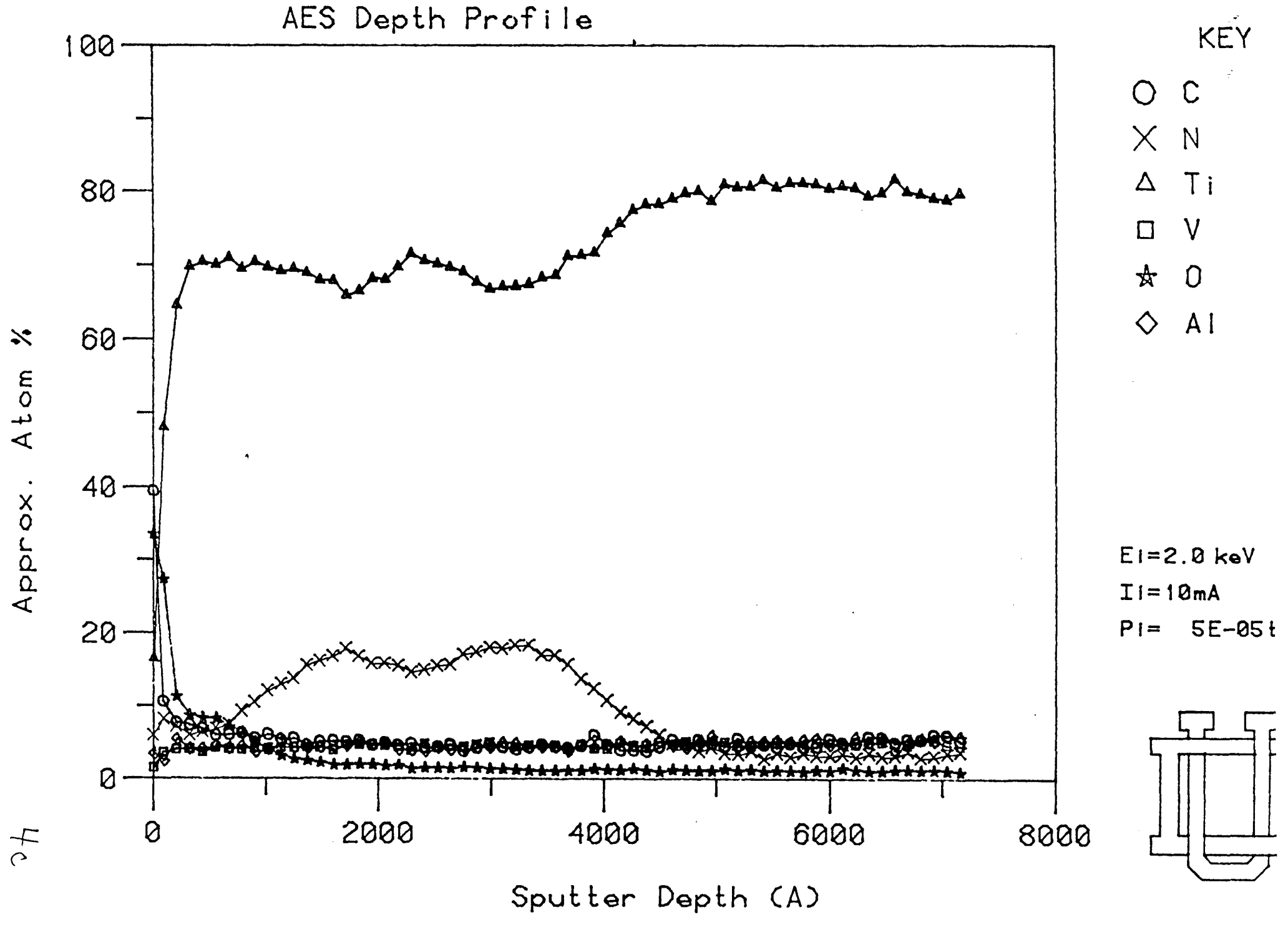

File: 062288.A08

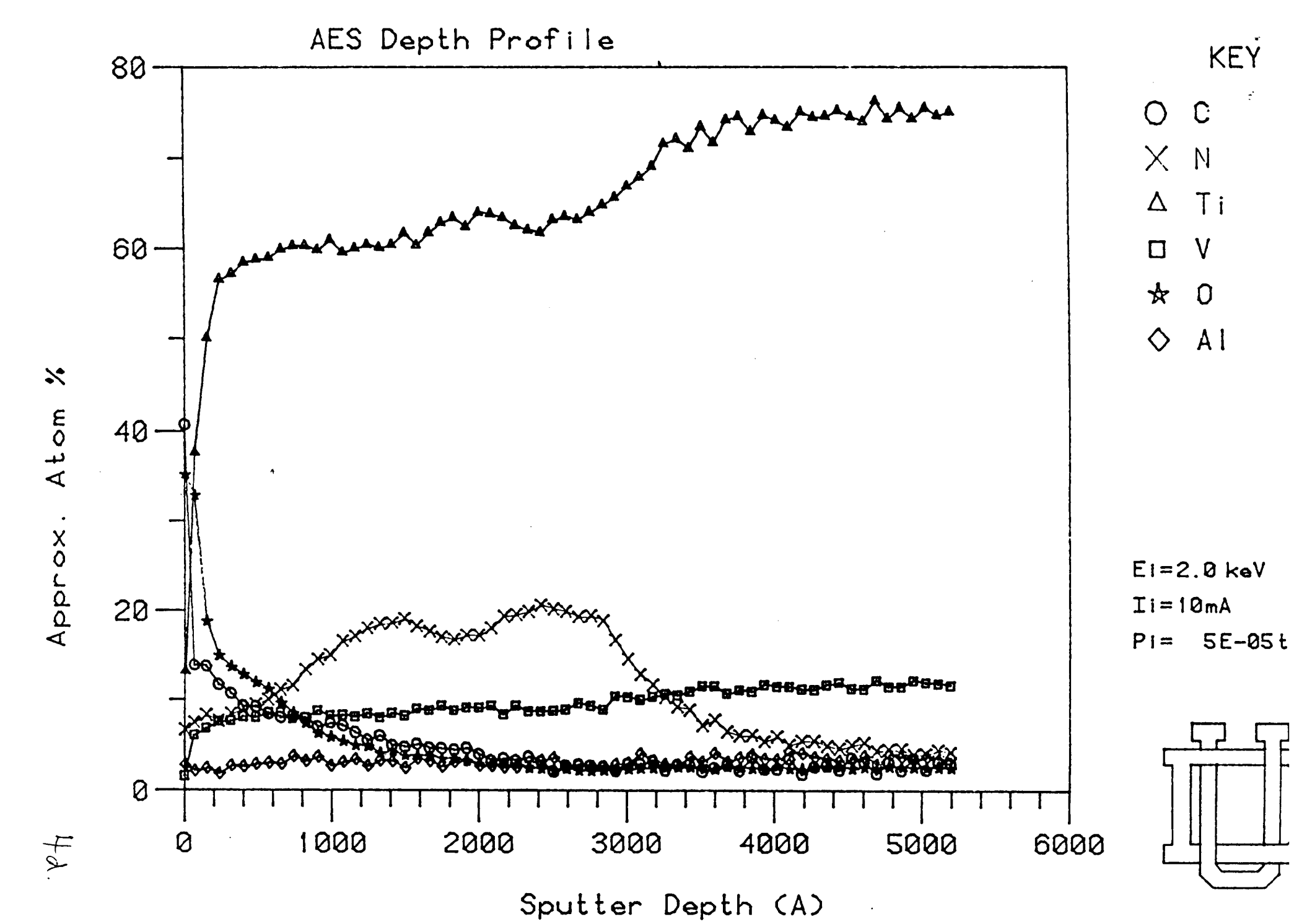

File: 062388.a02

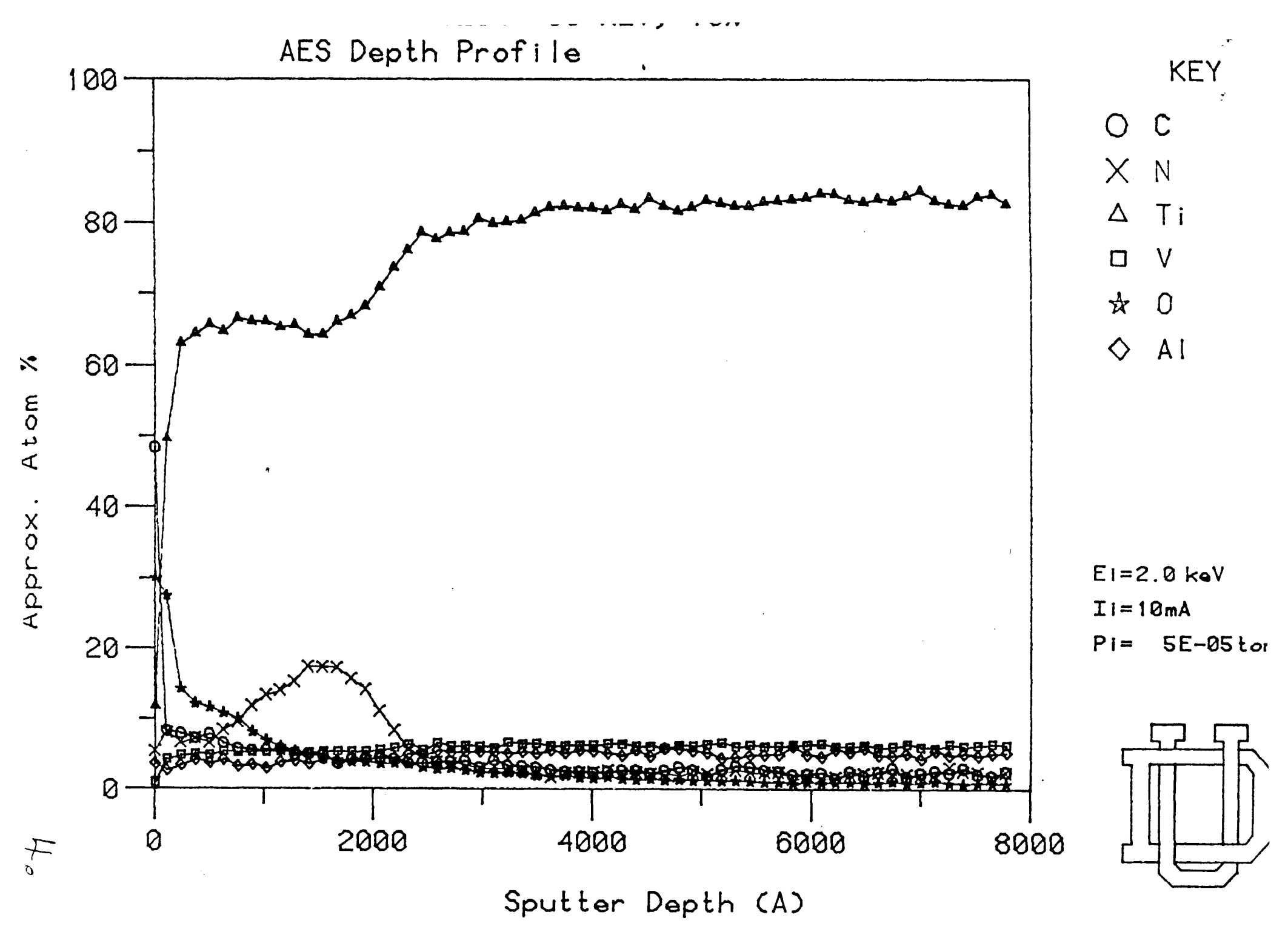

ile: 062488.A02

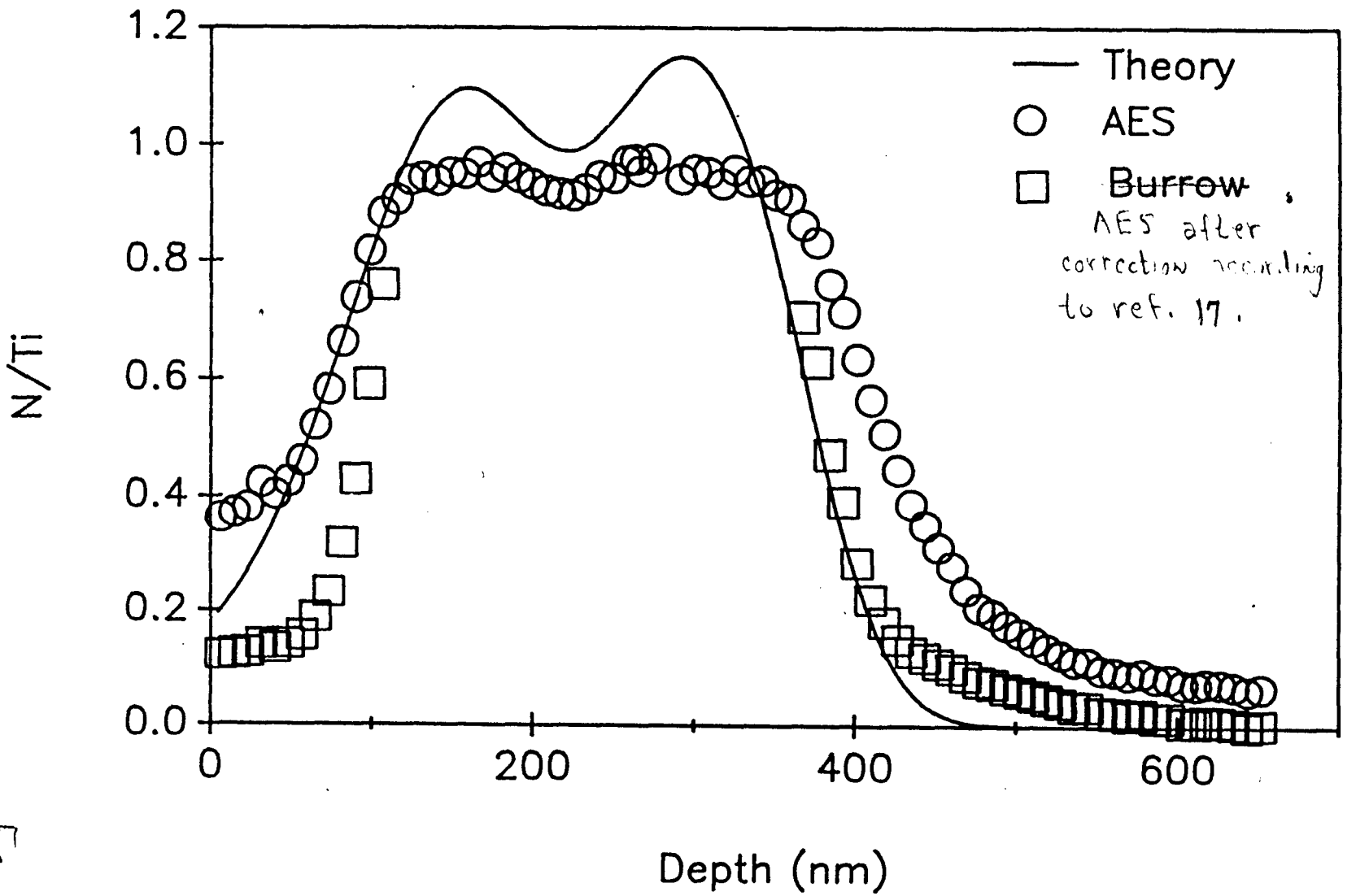
1.2
1.0
0.8
0.6
0.4
0.2
0.0
N/Ti
0
200
400
600
Depth (nm)
Theory
AES
Burrow
AES after correction according to ref. 17.

5a.

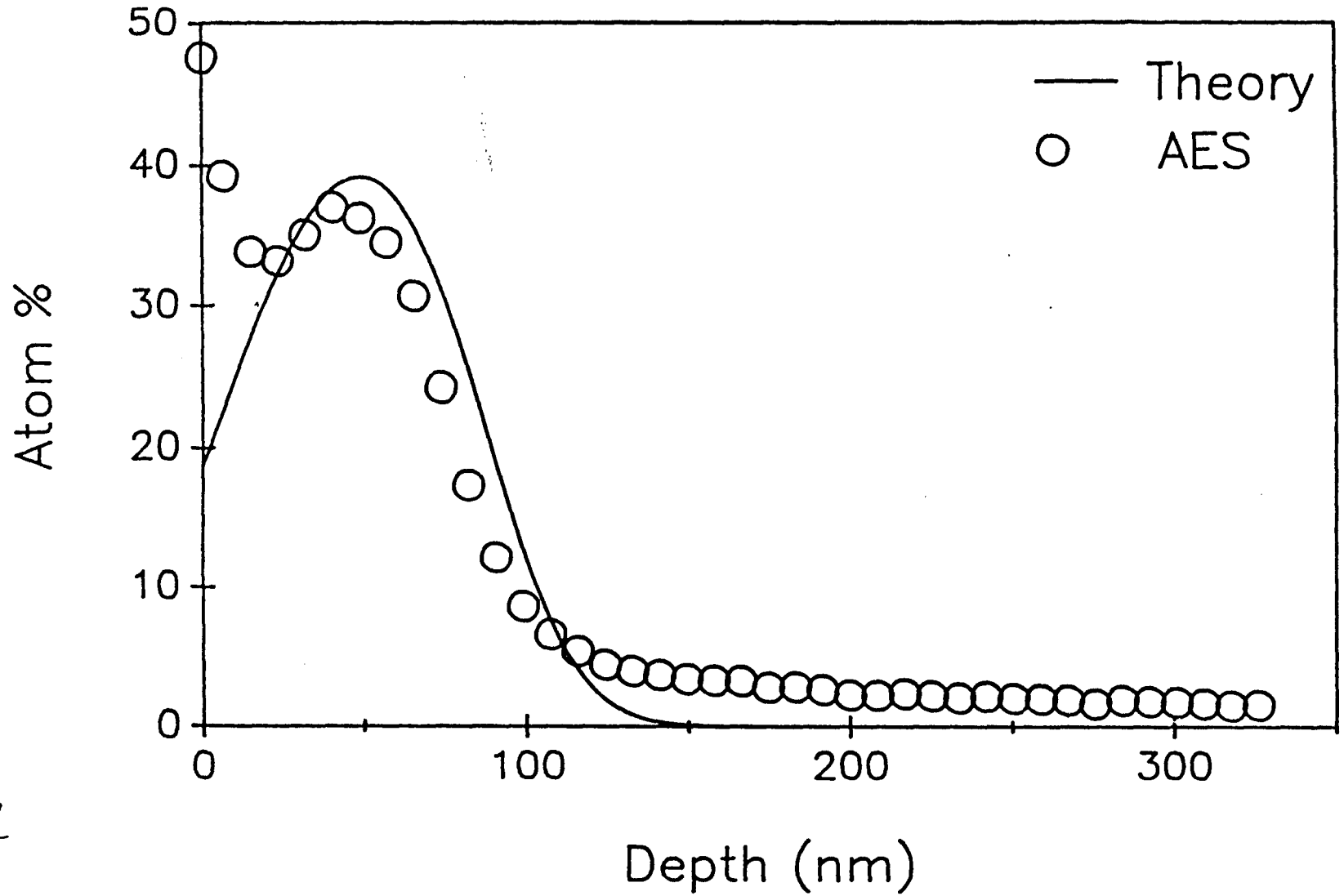
Theory
AES
Atom %
Depth (nm)
0
10
20
30
40
50
0
100
200
300

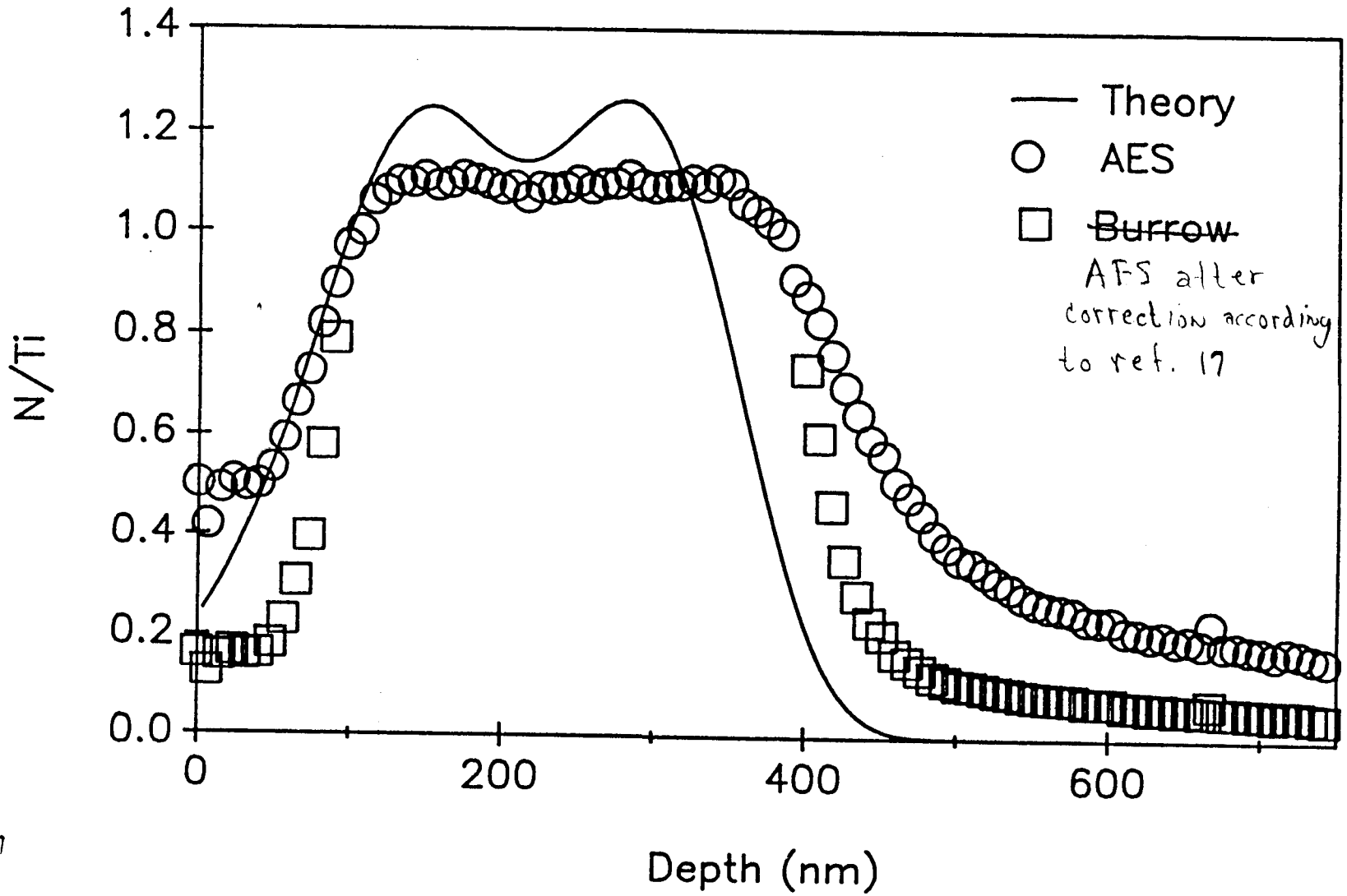
1.4
1.2
1.0
0.8
0.6
0.4
0.2
0.0
N/Ti
0
200
400
600
Depth (nm)
Theory
AES
~~Burrow~~
AFS after correction according to ref. 17

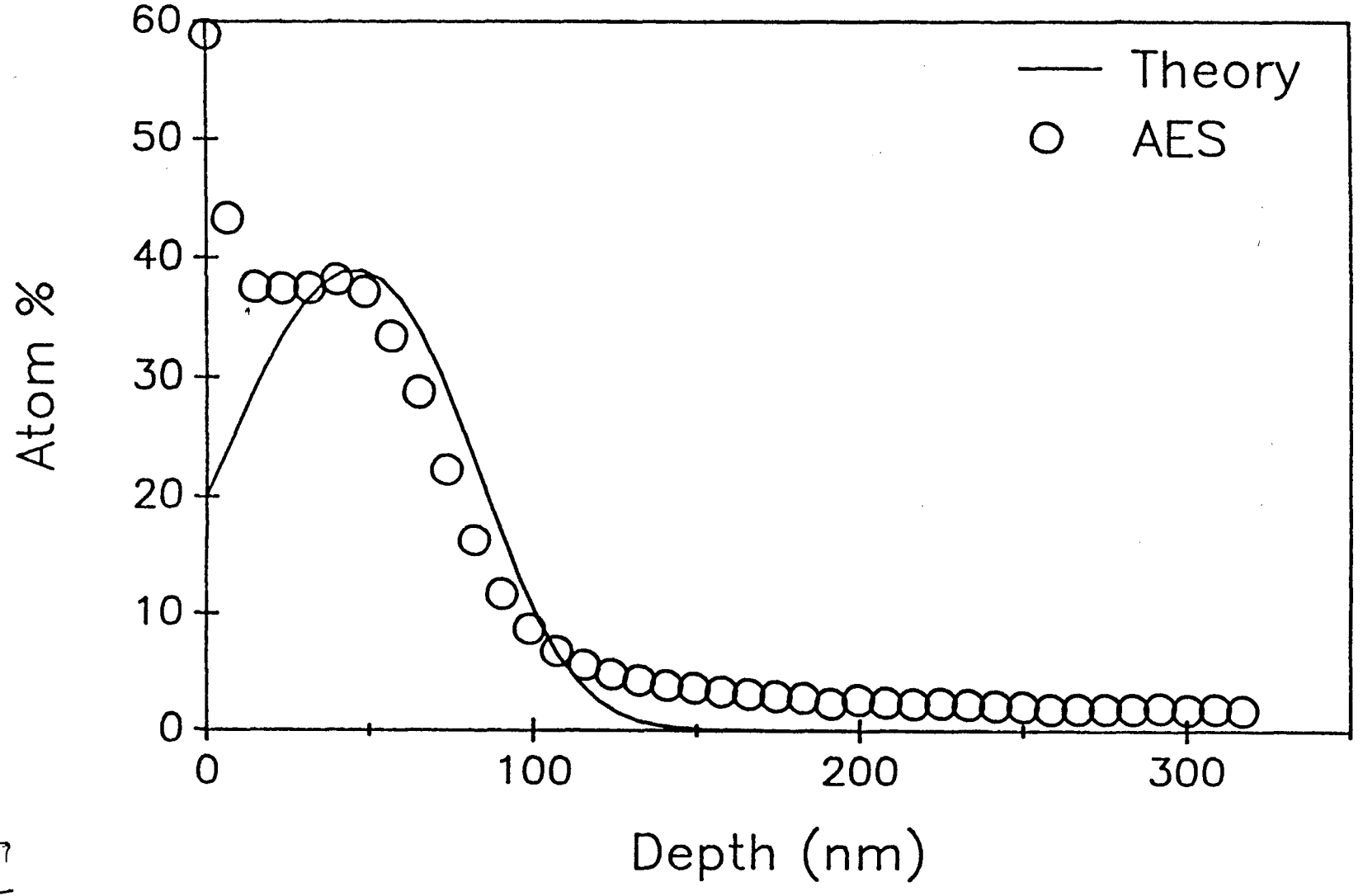
Theory
AES
Atom %
Depth (nm)
60
50
40
30
20
10
0
0
100
200
300

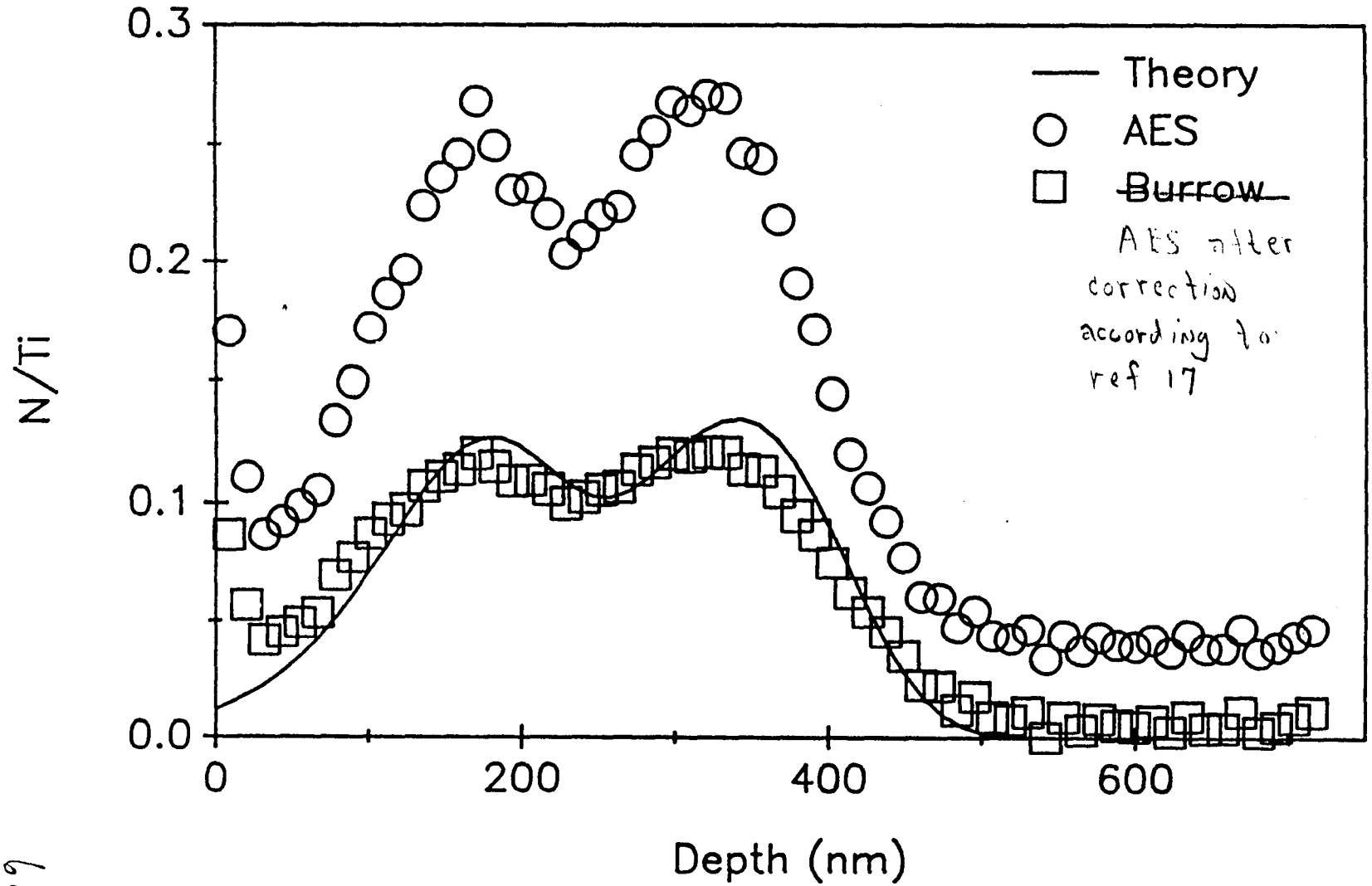
0.3
0.2
0.1
0.0
N/Ti
0
200
400
600
Depth (nm)
Theory
AES
Burrow
AES after correction according to ref 17

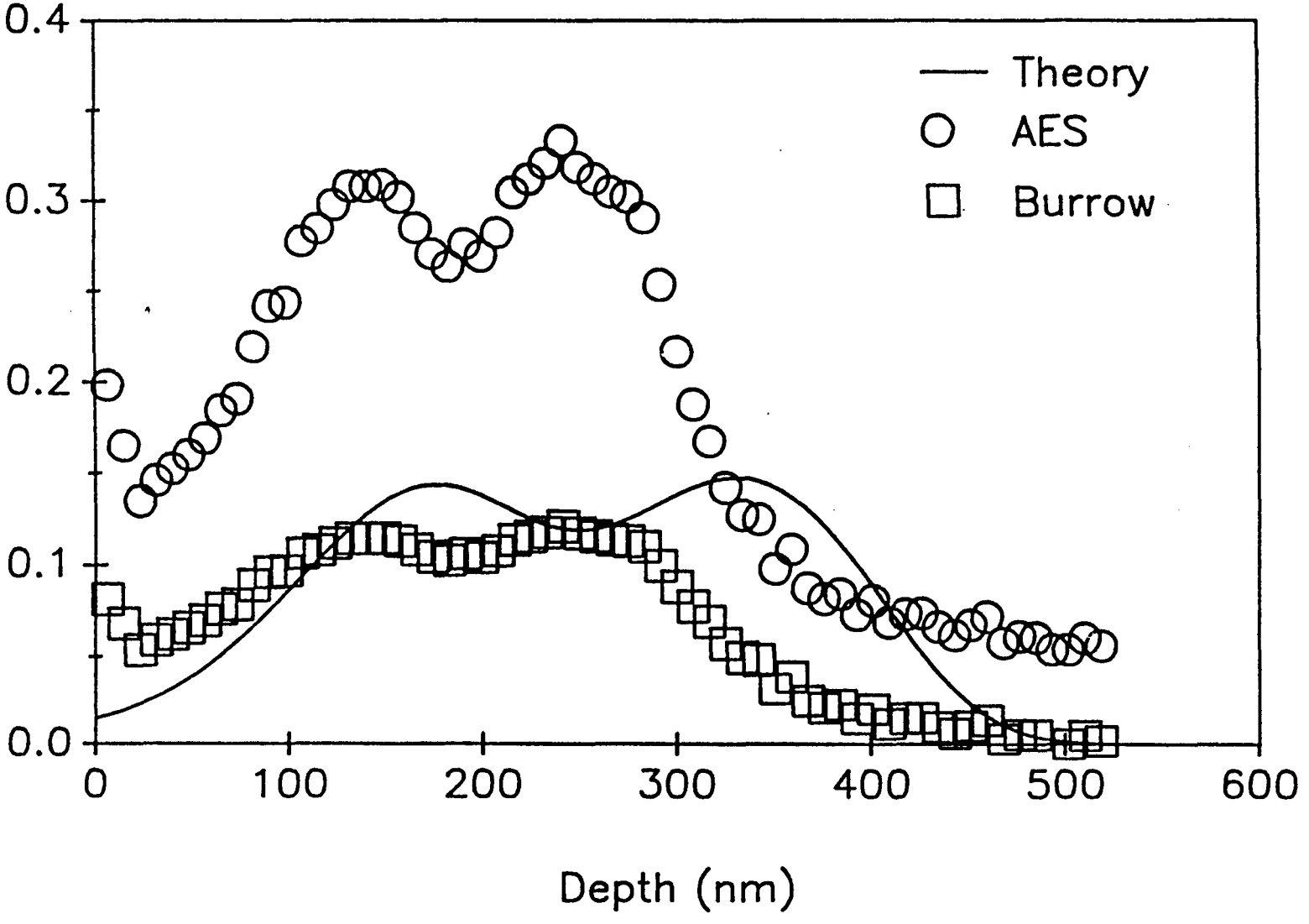
0.4
0.3
0.2
0.1
0.0
N/Ti
0
100
200
300
400
500
600
Depth (nm)
Theory
AES
Burrow

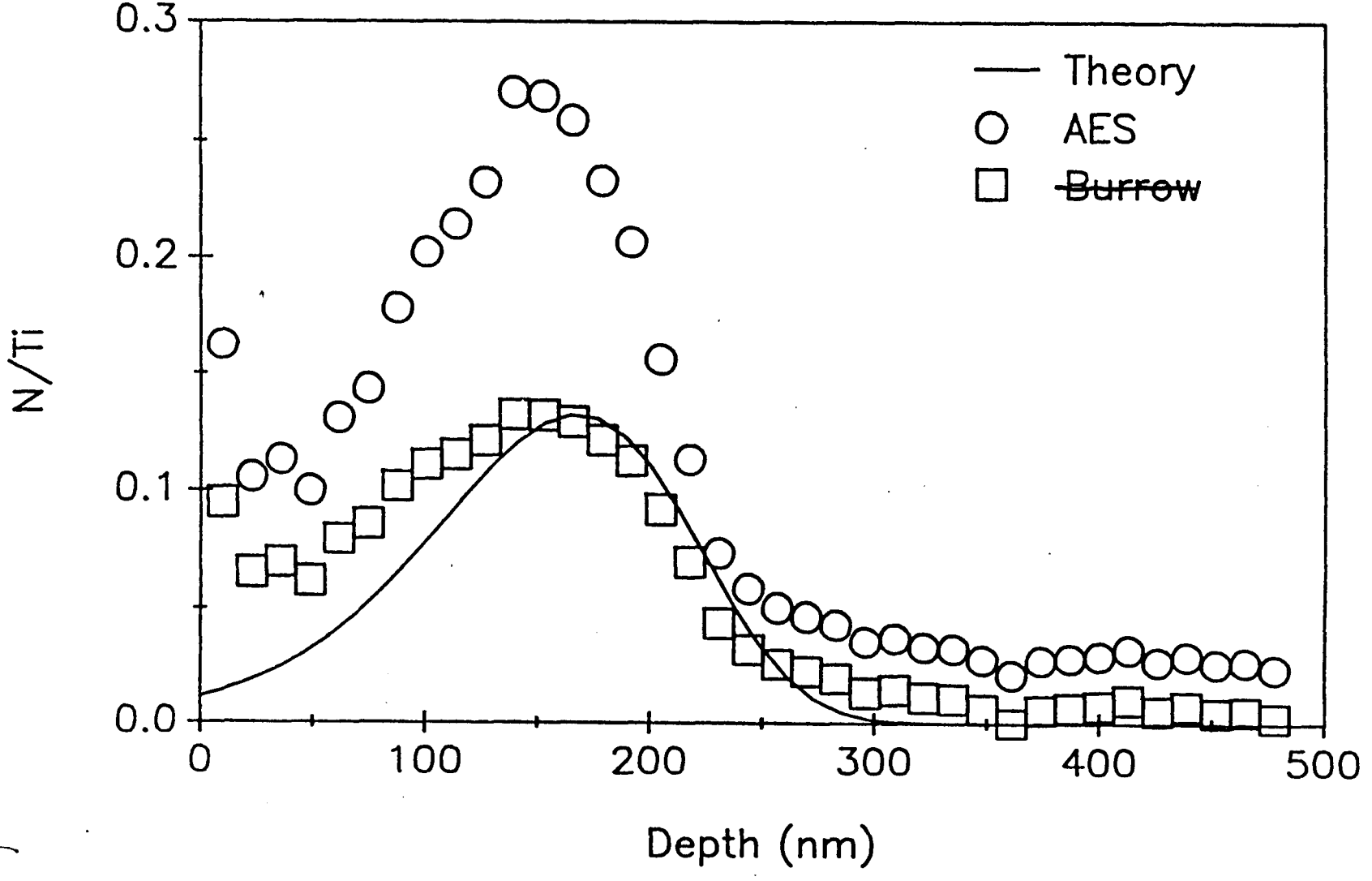
0.3
0.2
0.1
0.0
N/Ti
0
100
200
300
400
500
Depth (nm)
Theory
AES
Burrow